

# High-Field Dipolar Electron Paramagnetic Resonance (EPR) Spectroscopy of Nitroxide Biradicals for Determining Three-Dimensional Structures of Biomacromolecules in Disordered Solids

Anton Savitsky,<sup>\*†</sup> Alexander A. Dubinskii,<sup>‡</sup> Herbert Zimmermann,<sup>§</sup> Wolfgang Lubitz,<sup>†</sup> and Klaus Möbius<sup>†,||</sup>

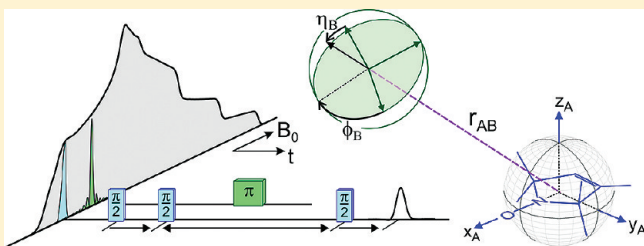
<sup>†</sup>Max-Planck-Institut für Bioanorganische Chemie, 45470 Mülheim an der Ruhr, Germany

<sup>‡</sup>Semenov Institute of Chemical Physics, 119991 Moscow, Russia

<sup>§</sup>Max-Planck-Institut für Medizinische Forschung, Abt. Biophysik, 69120 Heidelberg, Germany

<sup>||</sup>Department of Physics, Free University Berlin, 14195 Berlin, Germany

**ABSTRACT:** We consider the state-of-the-art capabilities and future perspectives of electron-spin triangulation by high-field/high-frequency dipolar electron paramagnetic resonance (EPR) techniques designed for determining the three-dimensional structure of large supra-molecular complexes dissolved in disordered solids. These techniques combine double site-directed spin labeling (SDSL) with orientation-resolving pulsed electron–electron double resonance (PELDOR) spectroscopy. In particular, we appraise the prospects of angular triangulation, which extends the more familiar distance triangulation. As a model case for spin-labeled proteins, the three-dimensional structures of two nitroxide biradicals with rather stiff bridging blocks and deuterated nitroxide headgroups have been derived. To this end we applied 95 GHz high-field electron dipolar EPR spectroscopy with the microwave pulse-sequence configurations for PELDOR and relaxation-induced dipolar modulation enhancement (RIDME). Various specific spectroscopic strategies are discussed to overcome the problems of overlapping spectra of the chemically identical nitroxide labels when attached to macromolecular systems. We conclude that due to the high detection sensitivity and spectral resolution the combination of SDSL with high-field RIDME/PELDOR stands out as an extremely powerful tool for 3D structure determination of large disordered systems. The approach compares favorably with other structure-determining magnetic-resonance methods. This holds true both for stable and transient radical-pair states. Angular constraints are provided in addition to distance constraints obtained for the same sample. Thereby, the number of necessary distance constraints is strongly reduced. Since each measurement of a distance constraint requires an additional doubly spin-labeled sample, the reduction of necessary distance constraints is another appealing aspect of orientation-resolving EPR spin triangulation for protein structure determination.



## 1. INTRODUCTION

The determination of a protein structure is of fundamental importance in bioinformatics as the shape of a protein strongly defines its biological functioning. Besides X-ray crystallography, NMR (nuclear magnetic resonance) spectroscopy is a prominent technique capable of revealing the structures of macromolecules such as proteins to atomic resolution. In addition to liquid-phase NMR, solid-state NMR is currently gaining more and more attraction, despite its inherent disadvantage of rather low sensitivity.<sup>1–3</sup> EPR (electron paramagnetic resonance) spectroscopy, on the other hand, is principally more sensitive than NMR by 6 orders of magnitude but is restricted to paramagnetic systems, such as naturally occurring redox reaction intermediates and metallo-proteins or artificially prepared spin-labeled complexes. Both NMR and EPR structure determination is based on measuring the dipole–dipole interaction of two magnetic moments of nuclear and/or electron spins. The dipole–dipole interaction frequency is a function of the interspin distance,  $r$ , and the orientation of the magnetic moments with respect to the external magnetic field. In the point-

dipole approximation this function is given by  $(1 - 3(\mathbf{d}, \mathbf{h})^2)/r^3$  with  $\mathbf{d}$  and  $\mathbf{h}$  being the interspin axis and external magnetic field directions, respectively.

Most commonly, solely distances are deduced from measured values of the dipole–dipole interactions between deliberately chosen sites of spin pairs. From these values, distance constraints can be constructed which have to be fulfilled by the macromolecule. If, however, also the orientation-dependent part of the dipole interaction could be measured, additional angle constraints would become available from the same sample. This would lead to a higher accuracy or faster convergence of the intricate procedure searching for the correct structure.<sup>3,4</sup> Moreover, the orientational constraints may provide information about the absolute position of the site in the laboratory frame of reference. Distance measurements, on the other hand, can generally provide only

**Received:** July 18, 2011

**Revised:** August 31, 2011

**Published:** August 31, 2011

relative constraints, that is, the distance of one site in the protein with respect to a second site. An important additional strength of magnetic-resonance methods, be it NMR or EPR, is their capability to study time-dependent phenomena, such as intramolecular dynamics in macromolecules, conformational changes in the course of a biological process, reaction kinetics, molecular recognition, or protein folding. Naturally, NMR technique samples much slower correlation times of motions<sup>5</sup> than EPR does.

Many proteins and other biocomplexes are available only as disordered samples, for example, frozen solutions. In this situation high-resolution X-ray crystallography is not applicable. As a potential resort, NMR and EPR methods offer powerful tools to obtain structural information over wide distance ranges depending on which dipolar spin interaction (nuclear–nuclear, electron–nuclear, electron–electron) is measured. By applying EPR methods, well-established techniques like FRET (fluorescence resonance energy transfer)<sup>6</sup> or solid-state NMR<sup>2</sup> are complemented concerning the accessible distance ranges. For dipolar electron–nuclear hyperfine interactions, preferentially measured by ENDOR (electron–nuclear double resonance) or ESEEM (electron spin echo envelope modulation), the accessible distance range stays well below 1 nm. For the dipolar electron–electron spin interaction as measured, for instance, by PELDOR (pulsed electron–electron double resonance) or RIDME (relaxation-induced dipolar modulation enhancement), the distance range can be extended dramatically, in ideal cases to about 8 nm.<sup>7</sup> For sufficiently large distances, say >1.5 nm, between well-localized electron spins A and B in a weakly coupled spin pair, the exchange coupling,  $J$ , can be neglected, and the point-dipole approximation holds. The detection sensitivity of the dipolar methods is determined by the squared dipole moment strength, thus strongly favoring EPR over NMR when the available sample volume is limited.

The success story of site-directed spin labeling (SDSL) of proteins by introducing paramagnetic nitroxide side chains and, moreover, combining SDSL with pulsed EPR dipolar spectroscopy<sup>8–12</sup> (abbreviated DS-EPR in the following) has inspired numerous structural studies of doubly spin-labeled protein complexes in disordered solids. DS-EPR is based on the spin–echo detection of EPR responses for which the pulse trains are tailored to carry information on the electron–electron dipolar interaction. Combined SDSL+DS-EPR studies require that pairs of interacting electron spin labels are attached to specifically chosen molecular sites of the complexes. Standard continuous wave (cw) EPR on spin labels in disordered solids is not suitable for distance measurements any more if the spin-pair separation exceeds a few nanometers.<sup>13</sup> In this instance, the electron dipolar splitting becomes too small to be resolved in the inhomogeneously hyperfine-broadened EPR spectra. In contrast, pulse DS-EPR echo methods cancel unwanted inhomogeneous spectral contributions but retain the dipolar contributions with information on the three-dimensional molecular structure.<sup>14</sup>

Strategically, for a complete structure determination DS-EPR has to be applied to a sufficiently large number of samples with consecutively labeled pair sites. This allows one to locate the labeled domains step by step until a “mapping” of constraints between many molecular sites has been accomplished. This procedure is occasionally called “electron-spin triangulation” in analogy to geodetic triangulation.<sup>10,15</sup> Thereby, the location of a specific point (“target”) is determined by measuring the distance and directional angles to it from a predetermined reference point (“observer”) located in its coordinate system (“reference frame”).

Two types of triangulation routines are established, *radial* and *angular* triangulation. In 3D space, radial triangulation requires a nonplanar four-point reference basis as the apexes of a tetrahedron. For SDSL+DS-EPR, the base points are the spin-labeled sites, whose relative positions are defined via the lengths of the six tetrahedron sides, that is, the six distances measured between the respective labels. In terms of the SDSL+DS-EPR techniques this means that for each of the distance measurements,  $r_{AB}$ , a special sample has to be prepared in which the complex is selectively 2-fold labeled at the positions A and B. Obviously, for a complete radial triangulation of a protein quite a large set of selectively labeled protein double mutants is needed. Despite the laborious molecular biology procedure, radial electron spin-triangulation has been successfully executed for a few proteins; see for example refs 10, 15, and 16. However, the number of doubly labeled protein samples increases tremendously with increasing size of the protein when striving for structural constraints of sufficient accuracy. Not all of these designated sites may even be accessible for double mutations with subsequent spin labeling.

The minimum number of samples with doubly spin labeled molecules required for triangulation could drastically be reduced if one would measure not only the distances between the spin-label pairs, but also the angles describing their relative positioning and the pair-axis orientation in the molecular frame; in other words, if one would perform angular triangulation in addition to radial triangulation. Distance plus angular constraints can be deduced from the high-field dipolar EPR spectra of a particular doubly labeled sample, for example, by introducing nitroxide side chains and applying W-band (95 GHz) high-field EPR methodologies.

In 3D space, angular triangulation generally locates the target point B with respect to a coordinate system with the observer point A at its origin. The appropriate variables are the distance from A to B and the two polar angles which define the A–B direction. In the specific case of nitroxide SDSL+high-field DS-EPR, with a dominating anisotropy of the electron Zeeman interaction, one nitroxide label can serve as the base coordinate system (observer radical) with its origin assigned to the spin-density center of the NO<sup>•</sup> radical and with the base axes aligned parallel to the principal axes of its g-tensor. It is noted, however, that the employment of orientation-resolving SDSL+DS-EPR at high Zeeman fields seriously complicates the extraction of distances from the spectra of disordered samples. This is in contrast to low external magnetic fields such as in S-band or X-band EPR, that is, without orientational Zeeman selectivity, when distances can be routinely read out from the experimentally obtained Pake patterns.<sup>10,16,17</sup> It has to be pointed out, that for doubly nitroxide spin labeled systems partial information on radical-pair orientation can be retrieved even at low EPR frequencies: the EPR spectrum of nitroxide radical is no longer dominated by the electron Zeeman interaction but by the anisotropic nitrogen hyperfine interaction with an axially symmetric coupling tensor ( $A_{zz} > A_{xx} \approx A_{yy}$ ). This allows for a qualitative determination of the dipolar vector orientation with respect to the dominant anisotropy direction, as was demonstrated by Schiemann and co-workers.<sup>18</sup> In high-field SDSL+DS-EPR the situation for determining distance and orientation is simplified; then only changes of local structures during biological function are of interest. Conformational changes often occur only in specific regions of the protein complex when the biological process is passing through different intermediate protein states. Prominent examples of such conformational changes are linked to light-induced proton transfer in bacteriorhodopsin<sup>19</sup> and light-induced electron transfer in photosynthetic reaction centers.<sup>20,21</sup>

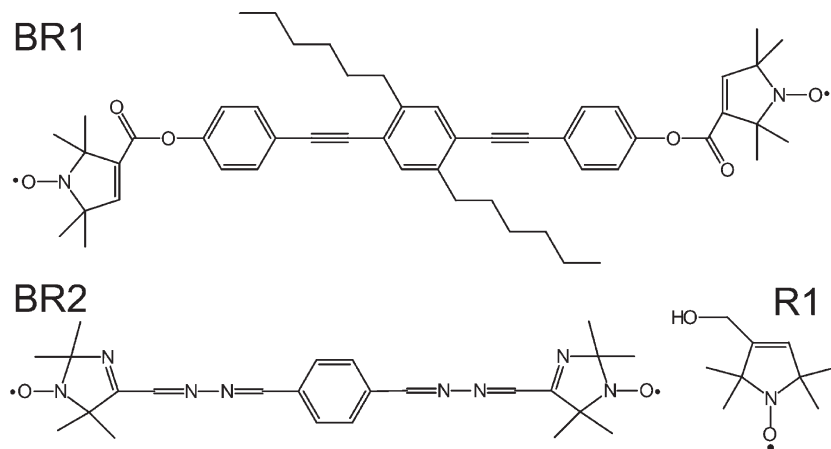


**Figure 1.** Molecular structures of nitroxide radicals R1 and biradicals BR1 (pyrroline type) and BR2 (imidazoline type).

In parentheses we note here that very recently W-band high-field pulse DEER (double electron–electron resonance) distance measurements on model systems and biological molecules have been reported for which Gd<sup>3+</sup> labels have been attached as electron spin probes, either instead of attaching nitroxide labels<sup>22–24</sup> or attaching a Gd<sup>3+</sup> label together with a nitroxide radical-pair partner.<sup>25</sup> Gd<sup>3+</sup> ( $S = 7/2$ ) containing tags as spin probes for distance measurements (without orientational selectivity) have attractive properties for high-field dipolar EPR: increased absolute detection sensitivity, localized electron spin on the Gd<sup>3+</sup>, isotropic  $g$ -factor, small zero-field splitting parameter, narrow and nearly isotropic width of the central EPR transition  $\Delta M_S = 1$  ( $| -1/2 \rightarrow |1/2\rangle$ ), fine-structure enhancement of the applied microwave field, and short spin–lattice relaxation times for rapid signal averaging. While double Gd<sup>3+</sup> spin labeling for DS-EPR based distance measurements has passed already the proof-of-principle test,<sup>22–24</sup> further studies of the spin physics and spin dynamics of Gd<sup>3+</sup> tags are needed to explore the advantages and limitations of this methodology for spin triangulation of large biosystems.

Returning to nitroxide double labeling for angular triangulation we emphasize that the biochemical/molecular biology synthesis program is minimized as compared to radial triangulation, but clearly at cost of an increased spectroscopic complexity in terms of high-field DS-EPR instrumentation and data analysis.<sup>20,26</sup> In this paper we consider typical problems encountered in orientation-resolving DS-EPR, and how to overcome them. We illustrate this by presenting W-band DS-EPR experimental results and their analysis for two specifically chosen nitroxide biradicals, BR1 and BR2. Their inter-radical separation is 2.9 and 2.0 nm, respectively, which is within the typical distance range for analogous studies of protein complexes. The biradicals have rather stiff bridging blocks which, however, still allow for residual conformational freedom of the nitroxide headgroups. Rigid bridging blocks minimize the distribution functions of distance and orientation of the spin labels relative to each other.<sup>27</sup> Such distributions contain additional structural information, but they often cause distortions of the spectra, complicate their analysis, and reduce the accuracy of the structural data.

## 2. MATERIALS AND METHODS

**2.1. Materials.** The biradicals BR1 and BR2 as well as the monoradical R1 used in this study are shown in Figure 1. Their synthesis and purification had been described previously: BR1 in

refs 27 and 28, BR2 in ref 29, and R1 in ref 30. For minimizing unwanted effects of spin dynamics and optimizing spectral resolution, the nitroxide headgroups were fully deuterated. If needed, the NO nitrogens were additionally labeled as <sup>15</sup>N isotopes (BR1-<sup>15</sup>N, BR2-<sup>15</sup>N, R1-<sup>15</sup>N). The radicals were dissolved in benzene (Aldrich, puriss. grade) to obtain a parent solution for all sample preparations. This solution was mixed with powdered *ortho*-terphenyl (Fluka, puriss. grade), and the benzene solvent was evaporated under air. The resulting powder solution, containing 1 mM of each radical, was heated to 65 °C to become fluid for transfer into the sample quartz capillary (inner diameter = 0.6 mm). A glass-type solution was obtained by shock freezing the sample in liquid nitrogen. The cold sample was finally transferred into the precooled EPR cavity.

**2.2. Methods.** All EPR experiments were performed with a laboratory-built W-band spectrometer operating either in cw or pulse mode at an EPR frequency of about 95 GHz and an external magnetic field of about 3.4 T, as described previously.<sup>26,31</sup> For measurements at 180 K, the sample temperature was controlled by a nitrogen gas flow in the cryostat. A gold plated bronze TE011 cavity was used (loaded quality factor  $Q_L = 2400$  of the empty cavity; temperature independent in the range 80–290 K). CW EPR experiments were performed using low microwave power (<1  $\mu$ W) incident on the critically coupled loaded cavity ( $\omega_1 < 1.5 \times 10^5$  rad·s<sup>-1</sup>) to avoid saturation of the spin system. The external magnetic field was modulated at 8 kHz with an amplitude of 50  $\mu$ T.

Both pulse dipolar EPR methods used in the present work, RIDME and PELDOR, utilize the stimulated spin–echo pulse sequence (SSE) with three  $\pi/2$  pulses at frequency  $\nu_A$ , in resonance with the observer spins A, with the preparation-detection time interval  $\tau$  swept and the mixing time interval  $T$  fixed; see Figure 2. RIDME (Figure 2a) works without additional microwave-induced spin flip by a  $\pi$  pulse in resonance with the target spins B,<sup>32</sup> whereas in PELDOR such a  $\pi$  pulse is applied to induce B-spin flips between the second and third  $\pi/2$  pulse;<sup>20</sup> see Figure 2b. This PELDOR pulse sequence differs from the three-pulse PELDOR version first introduced by Milov et al.<sup>33,34</sup> and also differs from the widely at X-band used four-pulse constant-time PELDOR sequence introduced by Jeschke et al.<sup>35</sup> The reasons for choosing the stimulated spin–echo pulse sequence are given below.

If measured at resonance with the observer partner of the radical pair, the SSE signal becomes modulated at the dipolar interaction frequency provided the electron spin of the target

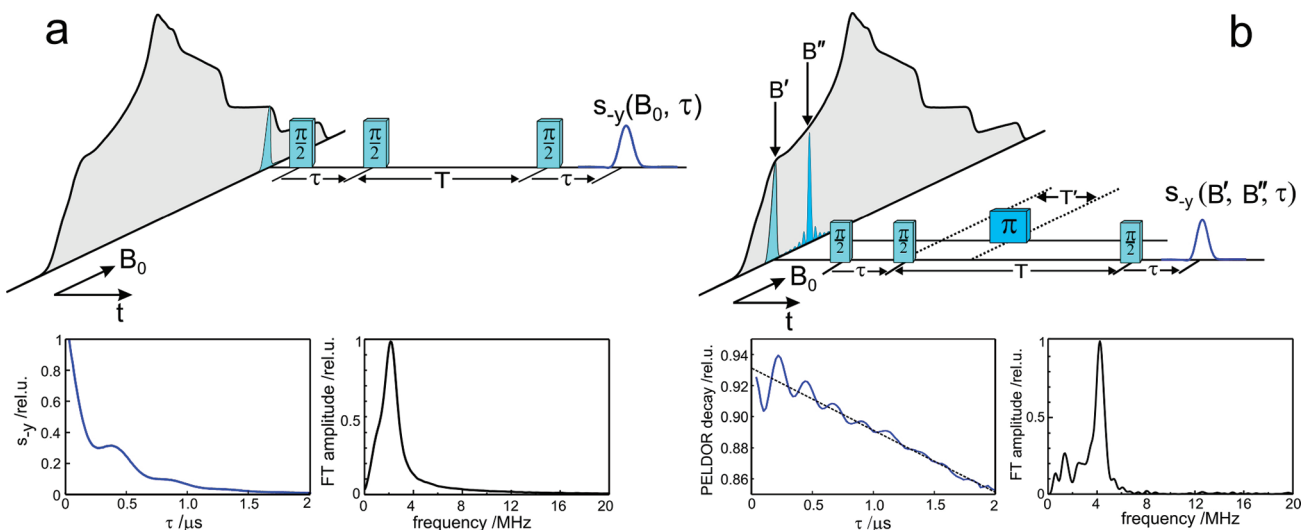


**Figure 2.** Top: W-band microwave pulse sequence for the (a) RIDME experiment and (b) dual-frequency PELDOR experiment on the nitroxide biradical BR1 in *ortho*-terphenyl solution at 180 K. The echo-detected EPR spectrum of BR1 and the microwave excitation bandwidth for typical microwave pulse-length settings are shown. (a) Typical settings are  $T = 33 \mu$ s,  $\pi/2$ -pulse length  $t_p = 30$  ns. The time  $\tau$  is stepped from  $\tau_0 = 30$  to 2000 ns in 10 ns steps. Bottom left: Representative example of a dipolar modulation echo-decay trace at the indicated magnetic field position. Bottom right: Fourier-transformed spectrum of the RIDME decay; the cutoff frequency of the high-pass filter was set to 1 MHz.  $B_0$  is the external magnetic field. (b) Typical settings are  $T = 5.6 \mu$ s,  $T' = 1.2 \mu$ s, and  $\pi/2$ -pulse length  $t_p = 32$  ns in the observer pulse sequence at frequency  $\nu_A$  (the observer spin and EPR-cavity resonance frequency). The pulse length of the additional  $\pi$ -pulse was adjusted to account for the mismatch of its frequency  $\nu_B$  (the target spin resonance frequency) from the resonance frequency  $\nu_A$  of the cavity. The preparation time  $\tau$  is varied from 50 to 2000 ns in 20 ns steps.  $B'$  and  $B''$  are resonance fields defined in the text. Bottom left: Representative example of a PELDOR decay trace (the ratio of echo amplitudes recorded with additional  $\pi$ -pulse on and off versus delay time  $\tau$ ). Bottom right: The Fourier-transformed spectrum of the PELDOR decay trace; the cutoff frequency of the high-pass filter was set to 1 MHz.

partner happens to flip over within the mixing period  $T$ . The RIDME method exploits the longitudinal relaxation with time constant  $T_1$  of the target spins which spontaneously induces the required spin flips.<sup>36</sup> The resulting RIDME responses, that is, the spin–echo amplitudes as a function of  $\tau$ , are sequentially acquired at magnetic field values that are stepped through the nitroxide EPR spectrum. They are then Fourier transformed with respect to the  $\tau$  dimension from the time to the frequency domain resulting in the 2D RIDME spectra,  $S_{\text{RIDME}}(\nu, B)$ . The fixed mixing time  $T$  has to be long enough to allow the longitudinal spin relaxation to flip the partner spins in the pair, but short enough to avoid a considerable reduction of the echo signal as a result of longitudinal spin relaxation and acceleration of the echo decay due to the spectral diffusion. The RIDME experiment, specifically when performed at high fields, is very sensitive to spectral diffusion and requires careful optimization of the experimental conditions, that is, sample temperature and concentration. Ultimately, a sample temperature must be found at which the echo decay parameters, that is, the phase memory time,  $T_m$ , the longitudinal spin relaxation time,  $T_1$ , and the inverse spin diffusion rate, are jointly optimized. For nitroxides in an *ortho*-terphenyl matrix, the optimum temperature for RIDME was found to be around 180 K. As an alternative to the temperature optimization for RIDME, the addition of fast-relaxing paramagnetic agents, for instance a holmium complex, was recently demonstrated to be able to tune the spin–lattice relaxation time,  $T_1$ , into the proper range.<sup>37</sup> To avoid additional  $T_2$  relaxation processes due to methyl group rotation at such an elevated temperature, the methyl groups of the nitroxide labels were deuterated.

In the PELDOR method, the required spin flips of the target radicals are coherently induced by a microwave  $\pi$  pulse in resonance with spins  $B$  during the mixing period  $T \ll T_1$ , in

addition to the observing three-pulse SSE train. This  $\pi$  pulse should not affect the observer spins; otherwise, distortions of the SSE response are caused, obscuring the dipolar spectra (see Section 4). There are two experimental strategies to excite and detect the spins in the different spectral regions; both of them are utilized in this work. The first strategy is dual-frequency PELDOR (DF-PELDOR)<sup>20,26</sup> where the measurements are made at a fixed value of the external magnetic field and two microwave sources are used. They are tuned to frequencies corresponding to the spectral positions selected for observing (resonance field  $B'$ , microwave frequency  $\nu_A$ ) and for pumping ( $B'', \nu_B$ ); see Figure 2a. The second strategy is field-jump PELDOR (FJ-PELDOR)<sup>26</sup> which selects the pairs of double-resonance positions by a magnetic field offset,  $\Delta B$ . In this case, a single microwave source is used, which is tuned to the cavity frequency (corresponding to  $\nu_A$ ). Right after the first two microwave  $\pi/2$ -pulses, the magnetic field is stepped rapidly (typically in less than 500 ns) from one position ( $B'$ ) within the EPR spectrum to another position ( $B'' = B' + \Delta B$ ) and then rapidly returned to  $B'$  during the precession-free period  $T$  of the stimulated echo sequence. The FJ-PELDOR method has the advantage to overcome the problem of the rather small excitation bandwidth of DF-PELDOR. This bandwidth is determined by the Q-limited cavity bandwidth and the rather small microwave power typically available at 95 GHz or even higher frequencies. Hence, FJ-PELDOR leads to an increased dipolar modulation depth, that is, to higher sensitivity. However, this sensitivity improvement limits the microwave pulse scheme for FJ-PELDOR to the stimulated echo (SSE) sequence. This is because any variation of the magnetic field during the development of spin coherence, that is, magnetization in the  $xy$  plane of the rotating frame, destroys the coherence and, thus, leads to a vanishing echo

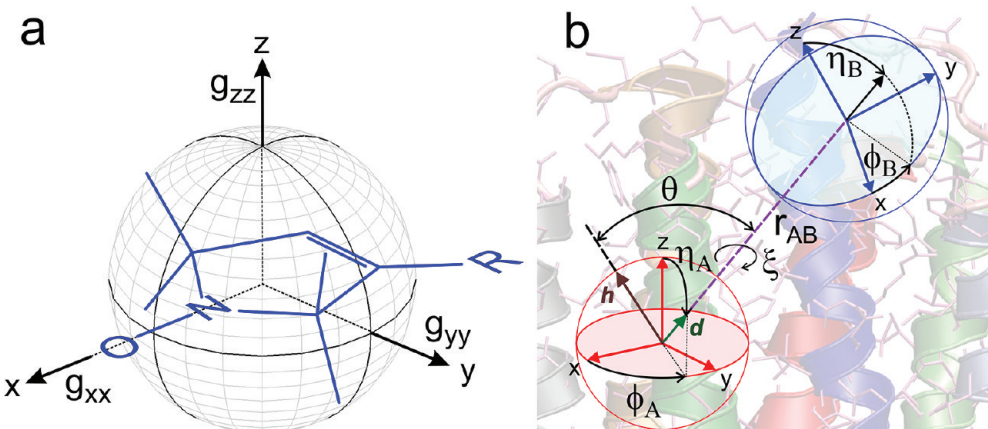


**Figure 3.** (a) Structure of the pyrroline type nitroxide fragment, definition of the  $g$ -tensor principal axes system in the unit sphere. (b) Definition of the radical-pair geometry parameters of radical A and radical B. The unity vectors  $\mathbf{h}$  and  $\mathbf{d}$  show the directions of the external magnetic field  $B_0$  and the dipolar interpair axis. For details, see the text.

observable. In the SSE sequence, the magnetization is stored along the  $z$ -axis (the direction of the external magnetic field) during the  $T$ -period, and hence, the additional jump field  $\Delta B$  does not affect the observed stimulated echo. Therefore, we generally choose the SSE sequence for both the DF- and the FJ-PELDOR experiments. Important details of the experimental settings, such as pulse duration, scan timing, and selection and sweep of the observer and target field positions, as well as the frequency stepping are given in the figures and figure captions (Figures 2, 4–9). The description of the hardware for the DF- and FJ-PELDOR methods, dead time, and related problems of data processing has been presented previously.<sup>20,38</sup>

### 3. SPECTROSCOPIC BACKGROUND

**3.1. Radical-Pair Geometry.** The relative positions of the radicals in the radical pair are characterized in coordinate systems that are suitably chosen for describing magnetic interaction parameters. The reference frames are attached to the molecular backbones as follows: The frame origins are fixed to the respective focal points of the electron spin density distributions in the radicals. Then, the spin–spin interaction of the electrons is treated in the point–dipole approximation. This is a good approximation for nitroxides separated by more than 1.5 nm. The frame axes are aligned parallel to the principal axes of the dominant anisotropic magnetic interaction in the radicals. For nitroxides in the high external magnetic field of a W-band EPR spectrometer, the anisotropy of the electron Zeeman interaction dominates all other molecular spin interactions. Consequently, the alignment of the magnetic reference frame coincides with that of the electronic  $g$ -tensor: The  $x$ -axis is along the N–O bond, and the  $z$ -axis is perpendicular to this bond and parallel to the nitrogen  $2p_z$  orbital (Figure 3a). The nitrogen hyperfine tensor ( $A$ -tensor) is assumed to be coaxial with the  $g$ -tensor,<sup>39</sup> which is justified for planar nitroxide radicals, for example, the five-membered-ring spin label used here.<sup>30</sup>

Either of the two nitroxide radical frames in the pair can be chosen as the triangulation base A (the observer radical), whereas the position of the second radical in the pair (the target radical B) is defined by the polar coordinates of its origin with respect to the reference frame A, that is, by the distance  $r_{AB}$  and the two polar angles ( $\phi_A$ ,  $\eta_A$ ). To complete this description, the alignment of

the second radical with respect to the base frame A is defined by the three Euler angles ( $\Phi_A$ ,  $\Theta_A$ ,  $\Psi_A$ ). Hence, the distance and five angles fully characterize the radical-pair structure. Since in any radical pair the observer and target radicals can be interchanged as reference frames, it is convenient to use, instead of two polar and three Euler angles, a redefined set of five independent angles that reflects the symmetry of the observer-target and target-observer frames.<sup>20</sup> Such angles are defined symmetrically with respect to both paired radicals and are more easily derived from an analysis of the dipolar EPR spectra. This set of angles includes the two pairs of polar angles, ( $\phi_A$ ,  $\eta_A$ ) and ( $\phi_B$ ,  $\eta_B$ ), which define the direction of the pair axis in the reference frame of nitroxide A and B, respectively. The last angle ( $\xi$ ) defines the turn of the paired radicals around the pair axis relative to each other; see Figure 3b. The two nitroxide radicals, when serving as mutual observers, have identical EPR spectra in disordered solids. Thus, their dipolar spectra overlap, and this complicates the analysis. Possible solutions of this problem are discussed below.

**3.2. Theoretical Considerations.** The theory of pulse dipolar EPR spectroscopy of weakly interacting radical pairs is well-described in the literature.<sup>9</sup> When applied to radical pairs, mathematical models and computational procedures have been developed that can be used for simulating multidimensional dipolar EPR spectra. The characteristics of the pair geometry serve as input parameters. They are amended by other input parameters which characterize the individual partner radicals of the pair, the experimental conditions as well as the pulse schemes actually chosen for the DS-EPR measurements.

For the simulation or synthesis of spectra, model calculations of dipolar radical-pair spectra are generally performed to assist the analysis of the recorded data. If the tested model structures are numerous and badly defined by their dipolar spectra, a visual comparison of calculated and experimental spectra does not help to select the correct solution. Then, a common option is to apply best-fit routines that minimize the overall (“global”) squared deviation between experimental and simulated spectra under variation of the geometry parameters. There is a caveat, however, for such a global fitting procedure: It is inherently non-transparent, as it operates with a large number of fixed and varied parameters.<sup>40–43</sup> Moreover, it suffers from the well-known problem that the solution is not unique: The global-fitting procedure

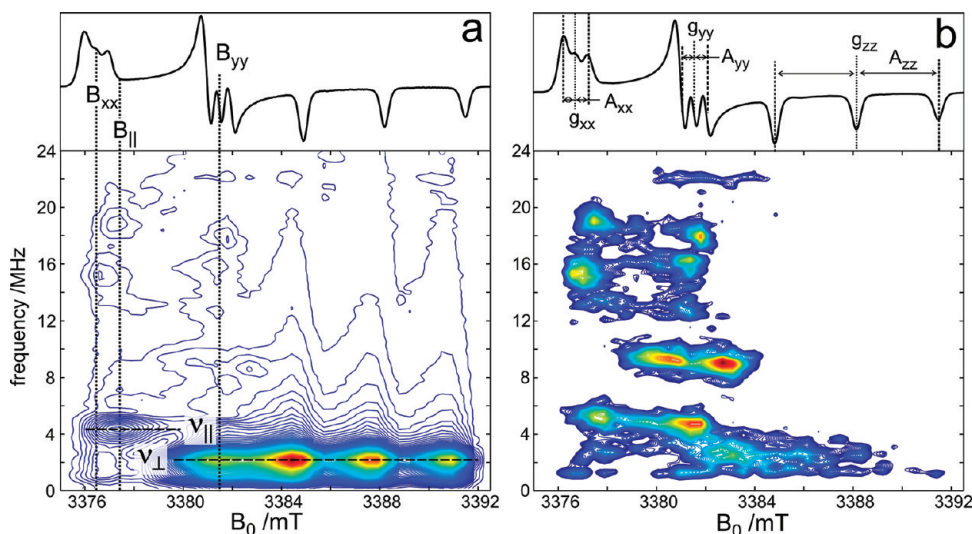


**Figure 4.** Fourier contour plots of the frequency-field dependence of the echo modulations observed by the RIDME pulse sequence ( $T = 33 \mu\text{s}$ ) applied to 1 mM nitroxide biradical BR1 (a) and monoradical R1 (b) in *ortho*-terphenyl glass at 180 K. The contour lines are shown as isohypses from 0.05 to 1 of the maximum FT RIDME intensity. The dashed lines in part a indicate the spectral regions of the canonical dipolar modulation frequencies  $\nu_{\parallel}$  and  $\nu_{\perp}$ . The  $g_{xx}$  and  $g_{yy}$  resonance field positions and field position of the  $\nu_{\parallel}$  response maximum are indicated by the dotted lines. On top, the corresponding experimental cw EPR spectra are shown. Note that the cw EPR spectra are practically identical, except for a slightly broadened  $g_{xx}$  component in the spectrum of BR1 due to the electron dipolar interaction.

hides intrinsic ambiguities of the spin-Hamiltonian solutions as well as potential correlations between the processed parameters.<sup>20,21</sup> In addition, any selective filtering which had been applied to correct experimental recordings has to be explicitly included in the simulations for a meaningful best-fit search. Otherwise, the minimization routine may converge to a fictitious solution that is without physical relevance.

As will be elaborated in the Results and Discussion section, echo-detected high-field EPR responses of nitroxides may show additional nuclear echo-envelope modulations that interfere with the dipolar echo modulations. They are caused by interactions between the unpaired electron and the nitrogen nucleus within the individual nitroxides. Hence, a clear understanding of the dipolar spectra of paired nitroxides is important to recognize their structure-related features and distinguish them from structure-irrelevant contributions. A deeper insight into the information content of orientation-resolving dipolar spectra of nitroxide pairs has been accomplished by considering model DS-EPR patterns that had been systematically simulated for a representative set of possible pair structures. The essential results of these simulations are as follows:

- For specifically oriented pairs with the dipolar axes declined from the magnetic field direction by an angle  $\theta$  (see Figure 3b) the dipolar spectrum is a doublet of lines located at the frequencies

$$\nu_{\pm} = \pm \nu_{\perp} (3 \cos^2 \theta - 1) \quad (1)$$

When summed over a uniform distribution of pair orientations with respect to the external magnetic field, spectral densities of dipolar modulations accumulate at specific frequency regions to constitute the famous Pake pattern.<sup>44</sup> They attain their maxima at  $\pm \nu_{\perp}$  and form steep edges at  $\pm 2\nu_{\perp}$ . Here, the principal dipolar frequencies,  $\nu_{\perp}$  and  $\nu_{\parallel} = |-\nu_{\perp}|$ , correspond to those radical pair orientations where the magnetic field is either perpendicular or parallel to the dipolar pair axis. For pairs of nitroxides in disordered solids,

an unperturbed Pake pattern can be detected only at relatively low EPR fields and frequencies with negligible orientation selectivity. The central hyperfine component  $M_1 = 0$  of the  $^{14}\text{N}$  nucleus should be selected for pumping in DS-EPR, because it is isotropic and accumulates uniformly the echo responses from all orientations.<sup>8,15</sup> The spacing between the principal features of the Pake pattern provides the intrapair distance,  $r_{AB}$ . Naturally, the angles that characterize the radical-pair orientation cannot be derived from such a powder-type spectrum.

- When the paired radicals exhibit a pronounced anisotropy of their dominant magnetic interaction, for example, the electron Zeeman interaction of nitroxides in W-band EPR, the dipolar spectral densities, as monitored at different field positions in the EPR spectrum, are selectively associated to observer radicals with different orientations and, thus, to differently oriented radical pairs.<sup>20</sup> Due to this orientation selection, the principal features of the Pake pattern become spread out over the field dimension and form characteristic singularities showing up as peaks and ridges in the spectra. Their coordinates on the field axis define the effective  $g$ - and hyperfine values. They can be analytically expressed via the principal values of the corresponding interaction tensors and the directional angles  $\phi, \eta$  of the magnetic field in the radicals' frames of reference. Hence, the angles  $(\phi_A, \eta_A)$  and  $(\phi_B, \eta_B)$  can be explicitly derived from the principal components of the  $g$ - and hyperfine-tensors—provided the respective canonical features are clearly resolved in the dipolar spectra.
- The fifth angle, the turning angle  $\xi$  in Figure 3b, does not affect the positions of the principal peaks in two-dimensional dipolar spectra when measured by a single-resonance experiment like RIDME. However, the angle  $\xi$  can be deduced from the analysis of PELDOR spectra.<sup>20</sup> Hence, a solution of the structure problem can be based on fitting the experimental PELDOR spectra by simulations with only one adjustable parameter  $\xi$ .

This fitting procedure is much better defined than a global multiparameter fitting. Moreover, when the principal singularities in the nitroxide dipolar spectra are well-resolved due to sufficient g-anisotropy, a solution of the structure may be derived without spectral fitting procedures.

## 4. RESULTS AND DISCUSSION

**4.1. RIDME Measurements.** The RIDME spectrum of biradical BR1 is shown in Figure 4a. In the frequency dimension it has maxima at  $2.14 \pm 0.05$  MHz and  $4.24 \pm 0.1$  MHz; they are assigned to the principal dipolar frequencies  $\nu_{\perp}$  and  $\nu_{\parallel} = |2\nu_{\perp}|$ . From the calibration relation  $\nu_{\perp} = 52.04(r_0/r)^3$  [MHz] ( $r_0 = 1$  nm),<sup>20</sup> the distance between the two nitroxide frames is deduced as  $r = 2.90 \pm 0.02$  nm. This is in good agreement with the distance obtained in a previous investigation of identical<sup>35,45,46</sup> or similar systems.<sup>17</sup> The perpendicular dipolar peaks at frequency  $\nu_{\perp}$  have field coordinates corresponding to the canonical  $g_{zz}$  value of the nitroxide EPR spectrum (the  $A_{zz}$  triplet of  $^{14}\text{N}$ , see the upper part of Figure 4b). This means that the radical-pair axis is normal to the  $z$ -axes of the two nitroxides, that is,  $\eta_A = \eta_B = 90^\circ$ .

The field value of the parallel dipolar peak is shifted from the canonical  $g_{xx}$  field toward that of  $g_{yy}$  EPR at this parallel field selects those orientations of the nitroxides for which the field director is tilted by the azimuth angle  $\phi_A$  (or  $\phi_B$ ) from the  $x$ -axis in the  $xy$  plane of radical A (or B). The orientation selection for the parallel dipolar coupling is given by the well-known relation<sup>47</sup> (which acts as an orientation selector):

$$g(\phi_A, \eta_A)^2 = (g_{xx}^2 \cos^2 \phi_A + g_{yy}^2 \sin^2 \phi_A) \sin^2 \eta_A + g_{zz}^2 \cos^2 \eta_A \quad (2)$$

For the radical-pair orientation, the dipolar interaction acts analogously to the Zeeman interaction; that is, it provides orientation selection by an external magnetic field. Thus, dipolar responses at the parallel frequency  $\nu_{\parallel}$  will show up at the “parallel” resonance-field position  $B_{\parallel}$  within the nitroxide EPR spectrum where the dipolar vector coincides with the direction of the external magnetic field. If the direction of the dipolar vector in the  $g$ -tensor frame is unique for all radical pairs detected, that is, for fixed  $\eta_A$  and  $\phi_A$  angles, the parallel dipolar response will appear at a unique parallel EPR resonance-field position

$$B_{\parallel} = \frac{h \cdot \nu_0}{g(\phi_A, \eta_A) \cdot \mu_B} \quad (3)$$

Taking into account that in the case of biradical BR1 the dipolar axis lies in the  $xy$  plane of the  $g$ -tensor frame, eq 2 can be simplified to

$$g_{xx}^2 \cos^2 \phi_A + g_{yy}^2 \sin^2 \phi_A = \left( \frac{\mu_B \cdot B_{\parallel}}{h \cdot \nu_0} \right)^2 \quad (4)$$

The numerical solution of eq 4 requires to know the  $g_{xx}$  and  $g_{yy}$  values as well as the values of the parallel resonance field and microwave frequency which, unfortunately, can only rarely be determined with high accuracy. However, taking into account the EPR resonance conditions for  $g_{xx}$  and  $g_{yy}$ , that is,  $h \cdot \nu_0 = g_{xx(yy)} \cdot \mu_B \cdot B_{xx(yy)}$ , the azimuth angle can be calculated from the

ratio of the resonance-field differences

$$\sin^2 \phi_A = \frac{B_{\parallel} - B_{xx}}{B_{yy} - B_{xx}} \quad (5)$$

This ratio can easily be determined from the EPR spectrum even without knowledge of the absolute magnetic field values, provided linearity of the magnetic field sweep is secured. In the BR1 case the field coordinate of the parallel dipolar peak is shifted by  $B_{\parallel} - B_{xx} = 1.0 \pm 0.2$  mT from the  $g_{xx}$  resonance-field position. The difference between the  $g_{xx}$  and the  $g_{yy}$  resonance fields,  $B_{yy} - B_{xx} = 5.1 \pm 0.2$  mT, was determined from RIDME recordings. It is in good agreement with the value 5.05 mT calculated by using the principal g-tensor components deduced from the cw EPR spectrum,  $[g_{xx}; g_{yy}; g_{zz}] = [2.00919; 2.00619; 2.00223]$ , and the experimental microwave frequency  $\nu_0 = 94.95$  GHz. Thus, from the resulting equation  $\sin^2 \phi_A = 0.19 \pm 0.02$ , the azimuth angle  $\phi_A = 26 \pm 3^\circ$  can be calculated.

Actually, this solution for the structure defines four symmetric variants of pair-axis alignment for which the axis (directed from the observer to the target) has azimuth angles of  $\phi_A(\phi_B) = 26^\circ, 180^\circ - 26^\circ, 180^\circ + 26^\circ$ , or  $360^\circ - 26^\circ$ , all of them satisfying eq 5. A choice between these variants can principally not be done by any EPR measurement alone<sup>20,21,47</sup> but requires additional independent information, for example, from X-ray crystallography.

As mentioned above, not only the RIDME electron dipolar mechanism contributes to modulations of stimulated spin-echo signals but also the hyperfine interactions between electron and nitrogen nuclear spins within the individual nitroxides of the radical pairs. As was shown previously, nitrogen nuclear ESEEM (electron spin echo envelope modulation) is clearly observable in W-band spin-echo decay signals of nitroxide radicals.<sup>30,48</sup> As a matter of fact, the three-pulse stimulated spin-echo (SSE) recordings, when acquired with the  $\tau$  interval fixed and the  $T$  interval swept (T-SSE mode), are well-suited for nuclear modulation studies, because they contain only modulations with the frequencies of nitrogen NMR transitions,  $\nu_{\alpha}$  and  $\nu_{\beta}$ , occurring within the  $\alpha$  and  $\beta$  electron spin manifolds of the nitroxide.<sup>49</sup> SSE recordings adjusted for electron dipolar modulation studies are commonly detected in the  $\tau$ -SSE mode ( $T$  interval fixed and  $\tau$  interval swept). They also contain nuclear modulation contributions at the frequencies  $\nu_{\alpha}$  and  $\nu_{\beta}$  and, in addition, at the combination frequencies,  $\nu_{\alpha} \pm \nu_{\beta}$ , which further complicates the spectrum analysis.<sup>49</sup>

The RIDME-type spectrum of the radical R1 is shown in Figure 4b. This pattern reveals nuclear spectral densities, that is, peaks and ridges, located mainly in the  $xy$  spectral region. The same features contribute also to the spectrum of biradical BR1; see Figure 4a. They are, however, dominated by more intense electron-electron dipolar contributions generated by the RIDME mechanism and are hardly discernible from the background noise level; that is, nuclear modulations do not prohibit an analysis of the dipolar RIDME spectrum.

A different situation is realized in the case of biradical BR2. The spectral-density representation of the modulated echo decays, recorded in the  $\tau$ -SSE mode, is shown in Figure 5a. This pattern is reminiscent of the RIDME spectrum in Figure 4a: The same triplet of peaks with the field coordinates around the canonical  $g_{zz}$  fields of the nitroxide spectrum indicates that the pair axis is directed perpendicularly to the  $z$ -axes of their nitroxide frames ( $\eta_A = \eta_B = 90^\circ$ ), similar to the BR1 case. The perpendicular

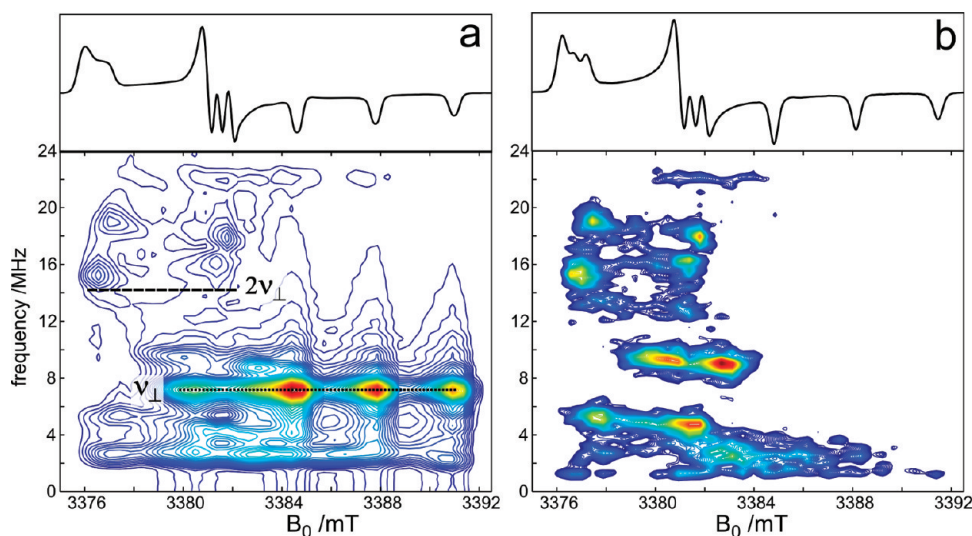


**Figure 5.** Fourier contour plots of the frequency-field dependence of the echo modulations observed by the RIDME pulse sequence ( $T = 33 \mu\text{s}$ ) applied to 1 mM nitroxide biradical BR2 (a) and monoradical R1 (b) in *ortho*-terphenyl glass at 180 K. The contour lines are shown as isohyps from 0.05 to 1 of the maximum FT RIDME intensity. The dotted line in part a indicates the spectral regions of the canonical perpendicular dipolar modulation frequency,  $\nu_\perp$ . The dashed line marks the frequency position  $2\nu_\perp$  at which the parallel dipolar response is expected. On top, the corresponding experimental cw EPR spectra are shown. Note that the cw EPR spectrum of BR2 shows significant line broadening of the  $g_{xx}$  and  $g_{zz}$  spectral components due to electron dipolar interaction.

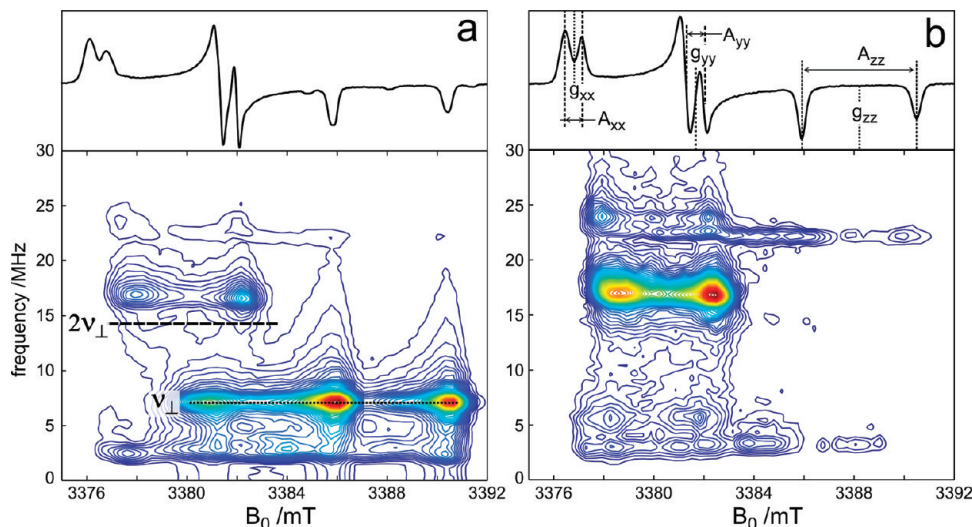


**Figure 6.** Fourier contour plots of the frequency-field dependence of the echo modulations observed by the RIDME pulse sequence ( $T = 33 \mu\text{s}$ ) applied to 1 mM BR2-<sup>15</sup>N nitroxide biradical (a) and R1-<sup>15</sup>N monoradical (b) in *ortho*-terphenyl glass at 180 K. The contour lines are shown as isohyps from 0.05 to 1 of the maximum FT RIDME intensity. The dotted line in part a indicate the spectral regions of the canonical perpendicular dipolar modulation frequency,  $\nu_\perp$ . The dashed line marks the frequency position  $2\nu_\perp$  at which the parallel dipolar response is expected. On top, the corresponding experimental cw EPR spectra are shown. Note that the cw EPR spectrum of BR2-<sup>15</sup>N shows significant line broadening of the  $g_{xx}$  and  $g_{zz}$  spectral components compared to R1-<sup>15</sup>N due to electron dipolar interaction.

dipolar frequency, as read out from these peaks, is  $\nu_\perp = 7.1 \pm 0.1$  MHz; it provides the interspin distance,  $r_{AB} = 1.94 \pm 0.01$  nm. This is in agreement with earlier distance estimates for this biradical from nonorientation-resolving X-band dipolar EPR.<sup>50–52</sup> In contrast to Figure 4a, the spectral pattern in Figure 5a between the canonical  $g_{xx}$  and  $g_{yy}$  fields is dominated by the nitrogen nuclear-ESEEM spectral densities. Taking their amplitude as a reference (see Figure 5b) the RIDME amplitudes of the well-resolved perpendicular peaks are reduced relative to those in Figure 4a. More significantly, the parallel dipolar peak expected

within the  $xy$  field region turns out to be greatly reduced and obscured by nitrogen ESEEM components. This makes it impossible to extract the coordinates of the parallel dipolar peak and to formulate the angular relations for  $\phi_A$  (and  $\phi_B$ ) which are required for solving the pair structure, as was done for BR1.

The reduction of the principal dipolar RIDME peaks of BR2 relative to BR1 is due to from RIDME line broadening which will severely reduce the dipolar peaks and may be caused by a distribution of the pair geometry parameters around their mean values. The distribution of interpair distances broadens the

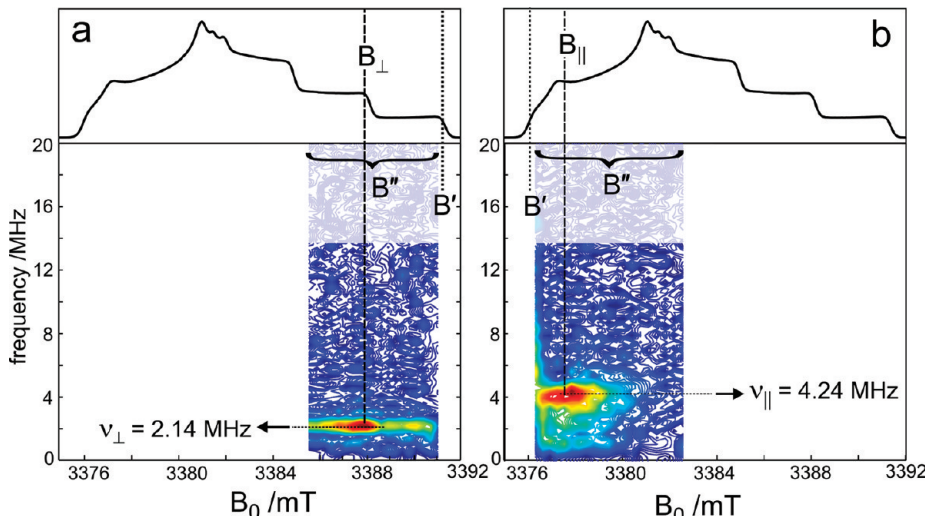


**Figure 7.** Dipolar dual-frequency PELDOR spectra of the BR1 nitroxide biradical (concentration 1 mM) in *ortho*-terphenyl glass at 180 K. The observer microwave frequency is fixed at a value corresponding to the resonance field  $B'$ , while the pump microwave frequency is swept through a region around the resonance frequency determined by the chosen field value  $B''$ . The contour plots show the Fourier amplitudes of the PELDOR echo-decay traces. On top, the corresponding experimental two-pulse echo-detected EPR spectra are shown, and spectral positions are indicated; see the text.

principal dipolar peaks in the frequency dimension.<sup>53</sup> This broadening grows with increasing dipolar frequency; that is, it will be larger for radical pairs with smaller interspin distances. For the parallel peaks it will be two times larger than for the perpendicular peaks. A distribution of the relative orientations of the pair partners will cause deviations of the pair axis from its mean direction: Hence, it will broaden the principal dipolar peaks in the field dimension.<sup>21,26</sup> Fortunately, both broadening contributions, distributions of distance and orientation, can be used to our advantage because they contain additional structural information on the molecular aggregates.<sup>21</sup> Our analysis shows that broadening of the dipolar peaks affects the  $\tau$ -SSE spectra of BR2 to a much greater extent than in the case of BR1. Thus, not surprisingly, the two model biradicals of our study reveal the most important requirement for 2-fold site-selective spin labeling for angular spin triangulation: The labels should be tethered to the molecular skeleton in a way which guarantees minimal scatter of both position and orientation.

Other unfavorable factors for structure determination concern specific features of nitroxide spectra. In fact, the parallel dipolar peak of BR2 is hardly discernible in Figure 5a because its expected frequency,  $v_{\parallel} = |2v_{\perp}| = 14.2$  MHz, is too close to the principal frequency ridge at  $v_{\alpha} = 15.0 \pm 0.1$  MHz at  $g_{xx}$  and  $16.1 \pm 0.1$  MHz at  $g_{yy}$  (see Figure 5b), which belongs to the  $^{14}\text{N}$  nuclear-ESEEM spectrum of the nitroxide radical.<sup>30</sup> In BR2, this ridge could be shifted away from  $v_{\parallel}$  after substituting  $^{14}\text{N}$  ( $I = 1$ ) for  $^{15}\text{N}$  ( $I = 1/2$ ). Unfortunately, after this substitution another intense nuclear-ESEEM ridge at the combination frequency  $(v_{\alpha} - v_{\beta}) = 16.9 \pm 0.1$  MHz is observed, approaching  $v_{\parallel}$ , thus obscuring the parallel dipolar peak; see Figure 6. The  $^{15}\text{N}$  nuclear-ESEEM components at  $(v_{\alpha} - v_{\beta})$  could be significantly reduced by accumulating the RIDME recordings over the properly stepped  $T$  interval, similar to what is done in the  $\tau$ -swept Mims-ENDOR experiment to avoid the blind spots.

An elegant solution to the problem of interfering nuclear-ESEEM contributions is available by extending the single-resonance experiment RIDME to the double-resonance experiment PELDOR. In the following we discuss the abilities of PELDOR to

resolve the sought-after parallel dipolar peak at  $v_{\parallel}$ , to provide the turning angle  $\xi$  (see Figure 3), and to further refine the solutions for the biradical structures.

**4.2. PELDOR Measurements.** Generally, PELDOR spectra represent the spectral density of dipolar modulation as a function of the dipolar frequency,  $\nu$ , and the two scanned spectral resonance-field positions,  $B'$  and  $B''$ , selected for the observer and target radicals. The spectral density, in turn, is derived by Fourier transformation of the measured echo-decay time traces to the frequency domain. Such 3D data arrays, that is, 4D geometry objects, cannot be displayed in their complete format. For visual inspection, their 2D data subsections, taken with one of the arguments fixed, can, however, be plotted. The PELDOR subspectrum of BR1, as shown in Figure 7a, was measured with the observer field position  $B'$  fixed to the high-field edge of the outer  $^{14}\text{N}$  hyperfine component. There the best orientational selection of the nitroxides is achieved; the selected biradicals are oriented with both their  $g$ -tensor  $z$ -axes parallel to the Zeeman field. The target spectral position was scanned by stepping the  $\pi$ -flip pulse frequency offset, counted from the fixed observer  $\pi/2$ -pulse frequency. For consistency with the field-domain presentation of spectral positions, the frequency offset was recalculated to the field offset:

$$B' - B'' = \frac{\hbar}{g \cdot \mu_B} \cdot (\nu_A - \nu_B) \quad (6)$$

The PELDOR spectrum in Figure 7a shows a distinct dipolar cross-talk at frequency  $v_{\perp}$  occurring between paired radicals with different nuclear spin states  $M_I = 0$  and  $-1$  (i.e., between different  $^{14}\text{N}$  hyperfine components) at the field position of the canonical  $g_{zz}$  component. Therefore, the orientations of the  $g$ -tensor  $z$ -axes for both paired radicals are parallel to the direction of the external magnetic field. This result reveals additional information: The  $z$ -axes of both nitroxide  $g$ -tensors are not only normal to the pair axis (see also the RIDME result above), but also parallel to each other, that is, the two nitroxide subunits of BR1 have a common  $xy$  plane and the symmetry related turning angles  $\xi = 0, 180^\circ$ . The additional PELDOR experiment in the  $xy$  spectral region, as in Figure 7b, allows one to validate the azimuth polar angle  $\phi$

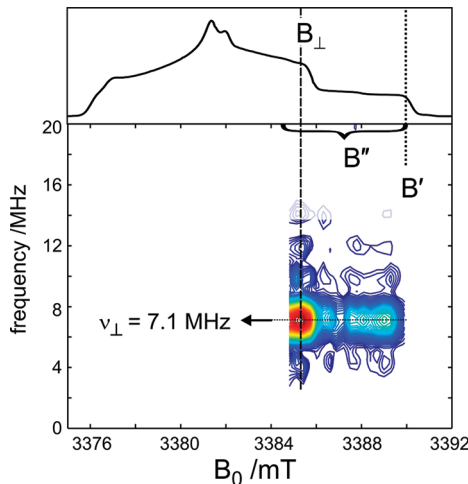


**Figure 8.** Dipolar dual-frequency PELDOR spectra of the BR2-<sup>15</sup>N nitroxide biradical 1 mM in *ortho*-terphenyl glass at 180 K. The observer microwave frequency is fixed at a value corresponding to the resonance field  $B'$ , while the pump microwave is swept through a region around the resonance frequency determined by the chosen field value  $B''$ . The contour plot shows the Fourier amplitudes of PELDOR echo-decay traces. On top, the corresponding experimental two-pulse echo-detected EPR spectrum is shown, and spectral positions are indicated; see the text.

deduced from RIDME. The radical-pair axis is tilted from the  $x$ -axes of the nitroxides by  $26 \pm 2^\circ$ . Importantly, the full set of radical pair geometry parameters:  $r_{AB} = 2.90 \pm 0.02$  nm,  $\eta_A = \eta_B = 90^\circ$ ,  $\phi_A(\phi_B) = 26 \pm 2^\circ$ , and  $\xi = 0$ , have been derived here solely from the dipolar EPR spectra, that is, without any a priori information about the biradical structure. In terms of distance and alignment of reference frames, this solution agrees well with the structure of BR1 in single crystals, as derived from X-ray crystallography.<sup>35</sup>

Our BR1 structure should be compared also with the results of a recent dipolar EPR study performed on a rather similar nitroxide biradical.<sup>54</sup> It differs from BR1 only by an additional aromatic segment within the inter-radical linking bridge. Thus, it exhibits a larger separation between the electron spins,  $r_{AB} = 3.86$  nm, and a correspondingly smaller principal dipolar frequency,  $\nu_\perp = 0.92$  MHz. However, both biradicals contain the same nitroxides, identically bonded to similar rod-like bridges and hence, analogous orientations of the radical-pair frames are expected. Polyhach and co-workers<sup>54</sup> considered two structure models for simulating their dipolar spectra of the biradical: Model 1 is based on the assumption that the terminal nitroxides can turn uniformly around the bridge axis (i.e., the mean dipolar axis) by any angle  $0 < \xi < 360^\circ$ , while their molecular  $z$ -axes (along the nitrogen  $2p_z$  orbital) are perpendicular to the bridge  $\eta_A = \eta_B = 90^\circ$ , and their molecular  $x$ -axes are tilted by  $25^\circ$  from the bridge direction. Model 2 is based on MD calculations, from which different biradical structures were derived together with their probabilities of realization. The dipolar spectra were simulated for these structures and weighted with their probabilities. It was found that model 2 shows a better agreement between the simulated and the experimental spectra. Since for the obtained biradical structure neither mean parameter values of distance and angles nor their dispersions are given in ref 54, we cannot make a quantitative comparison with our results. Qualitatively, we are in accord with the main message of the authors<sup>54</sup> that structural distortions and distributions of the biradical strongly affect

the dipolar spectra. The destructive impact of distributions of structural parameters on the dipolar spectra is also in line with our RIDME results of BR2 (see above).

The PELDOR spectrum of BR2-<sup>15</sup>N is shown in Figure 8, as obtained for the high-field  $g_{zz}$  region (analogous to that of BR1 in Figure 7a). The dipolar cross-talk between the <sup>15</sup>N  $A_{zz}$  hyperfine components ( $M_I = +1/2, -1/2$ ) occurs at the perpendicular frequency  $\nu_\perp = 7.1 \pm 0.1$  MHz, which is in agreement with the RIDME results. This shows that the  $z$ -axes of the nitroxides in BR2 are aligned almost parallel to each other, that is,  $\xi = 0, 180^\circ$ , analogous to BR1.

To discern the spectral position of the parallel dipolar peak in the  $xy$  field region corresponding to  $g_{xx}$  and  $g_{yy}$ , a series of FJ-PELDOR experiments was performed with some modification of the original scheme:<sup>38</sup> The external magnetic field was scanned to drive the fixed-frequency pulse sequence through the nitroxide EPR spectrum, while the resonance-field offset, the field jump  $\Delta B$ , between the observer and target spectral positions, was fixed consecutively to several sampling values. Each measurement then yields the 2D subarray data presentation, that is, the spectral densities of the SSE dipolar echo modulations versus the modulation frequencies and field positions; see Figure 9. This presentation of PELDOR data reminds one of RIDME spectra. The dipolar contributions to the PELDOR recordings are differentiated against contributions from nuclear-ESEEM and RIDME by the following experimental procedure: The  $\tau$ -SSE signals detected *without* the excitation microwave  $\pi$ -pulse, but keeping the field-jump pulse, that is, the signals carrying only nuclear-ESEEM and small RIDME contributions, are subtracted from signals detected *with* the complete PELDOR pulse train. In such a difference spectrum, the nuclear and RIDME modulation contributions cancel, whereas the dipolar modulation are preserved, provided the observer-target offset is large enough to prevent direct impact of the flip pulse on the observer spins. Otherwise, the difference can still contain the obscuring nuclear-ESEEM contribution.

An additional important factor may obscure the FJ-PELDOR spectrum. The reason is that the PELDOR pulse sequence, when based on the stimulated echo sequence, is conceptually similar to that used in HYSCORE (hyperfine sublevel correlation), but with the  $\pi$ -pulse being applied at a different spectral position. If the bandwidths of the excitation and observer pulse sequences do not overlap, the  $\pi$ -pulse only excites the forbidden EPR transitions; that is, it creates the nuclear coherences, which give rise to the induced nuclear modulations similar to that seen in the soft-ESEEM experiment.<sup>55</sup> In the case of DF-PELDOR, these modulations are washed out to a large extent by averaging the signal. This is because there exists no fixed phase relation between the observer and pump microwave fields which are typically generated by two independent microwave sources. FJ-PELDOR, on the other hand, uses the same coherent microwave field for both detection and excitation and, thus, will conserve the unwanted nuclear modulations.<sup>55</sup> Such an obscured FJ-PELDOR spectrum of BR2-<sup>15</sup>N is shown in Figure 9a. The field-jump was set to  $\Delta B = B' - B'' = 0.8$  mT, which corresponds to a frequency offset of 22.4 MHz. Significant nuclear modulations arise at the combination frequencies ( $\nu_\alpha - \nu_\beta$ ) around 17 MHz in the  $xy$  spectral region. An increase of  $\Delta B$  to 1.9 mT (53 MHz) suppresses the nuclear-ESEEM contribution owing to a minimized excitation overlap and the absence of sharp forbidden transitions. The spectrum reveals the otherwise hidden parallel cross peak, as is highlighted in Figure 9b. The exhumed parallel dipolar peak at  $\nu_\parallel = 14.2 \pm 0.2$  MHz is shifted by 2.4 mT from the  $g_{xx}$  field

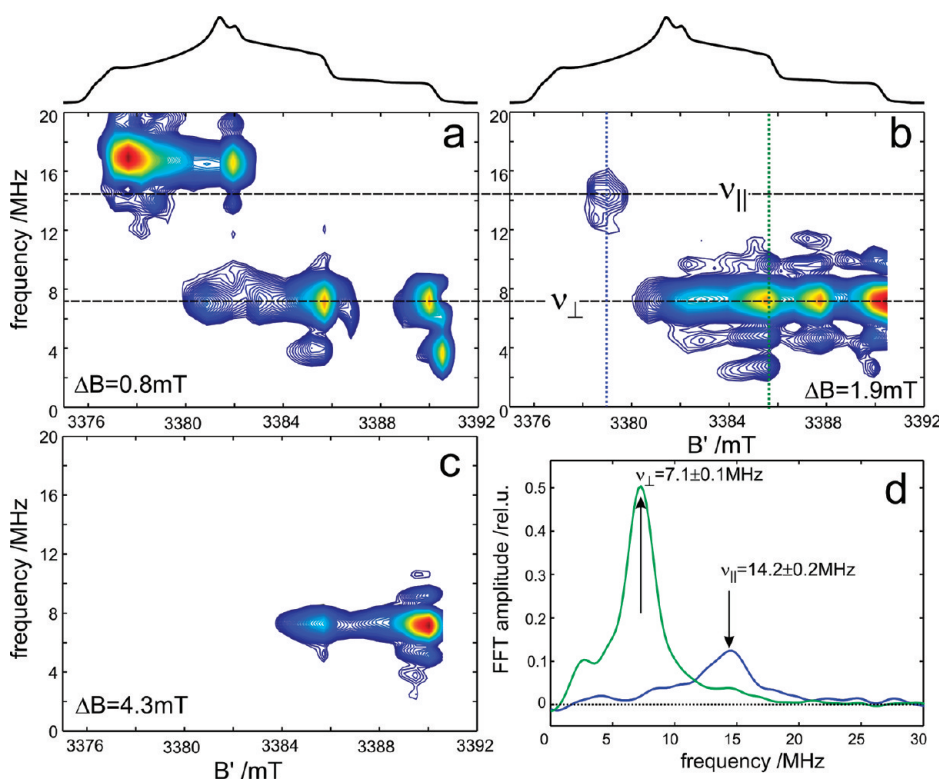


**Figure 9.** Dipolar field-jump PELDOR spectra of the BR2-<sup>15</sup>N nitroxide biradical 1 mM in *ortho*-terphenyl glass at 180 K. The spectra are acquired in the field-jump setting of the PELDOR experiment which differs from DF-PELDOR settings. The observer microwave frequency  $\nu_A$  is fixed at a value corresponding to the swept resonance field  $B'$ . The pump microwave pulse is also applied at  $\nu_A$  but at the magnetic field position  $B''$  during fixed amplitude ( $\Delta B = B' - B''$ ) field-jumps,<sup>38</sup> which is kept fixed for the experiment. The contour plots show the Fourier amplitudes of the PELDOR echo-decay traces for the different fixed  $\Delta B$  values: (a) 0.8 mT, (b) 1.9 mT, (c) 4.3 mT. On top, the corresponding experimental two-pulse echo-detected EPR spectrum is shown to refer to the spectral positions. (d) The frequency PELDOR spectra at the  $B'$  field positions indicated by dotted lines in panel b.

position. This frequency is twice the perpendicular frequency  $\nu_{\perp} = 7.1 \pm 0.2$  MHz, as measured in the  $z$  field region of the  $g$ -tensor using a  $\Delta B$  of 4.3 mT (120 MHz); see Figure 9c.

The biradicals BR2 and BR1 have a symmetric structure; therefore the parallel dipolar response is detected at the same field position within the EPR spectrum. Nevertheless, the nitrogen hyperfine splitting, which separates the EPR resonances of the observer and target nitroxides, allows for an independent pulse excitation of either the observer or target radicals.

For the isotope-labeled <sup>15</sup>N nitroxides with the external field  $B_0$  aligned within the  $xy$  plane, the nitrogen hyperfine splitting is about 0.72 mT (20.2 MHz). The magnitude of this hyperfine splitting rationalizes the offset value,  $\Delta B = 1.9$  mT, chosen for recording the PELDOR spectrum in Figure 9b: While the sampling SSE pulses at  $\nu_A$  are in resonance with the high-field <sup>15</sup>N hyperfine component of the observer radical, the spin-flipping  $\pi$ -pulse at  $\nu_B$  does not affect the observer radicals substantially, although it is still close enough to the low-field hyperfine component of the target radical to cause PELDOR modulations. A further increase of  $\Delta B$  draws the  $\pi$ -pulse frequency too much apart from the resonance frequency of the target radical-pair partner in the parallel alignment of the dipolar axis so that the parallel dipolar peak vanishes (see Figure 9c). Only when the field offset approaches the magnitude of the <sup>15</sup>N hyperfine coupling ( $A_{zz} = 4.52$  mT), distinct dipolar modulations appear again, but now at the perpendicular frequency  $\nu_{\perp} = 7.1$  MHz. They cause the cross peak at the canonical  $g_{zz}$  field position of the PELDOR pattern, as is shown in Figure 9c.

We see that the PELDOR techniques provide the complete set of dipolar spectra required for solving the pair geometry even in such unfavorable cases, when the spectra are heavily obscured by nuclear-ESEEM from the individual nitroxide radicals. The final solution for BR2, derived in the same way as for BR1, results in a pair structure with  $r_{AB} = 1.94 \pm 0.01$  nm, coplanar  $xy$  planes of both radical molecular frames, the pair axis located in this mutual plane, and the local  $x$ -axes tilted from the pair-axis direction by about 44°.

In principle, there exist two structure variants with different spatial symmetry that satisfy the solution obtained from dipolar EPR spectroscopy: One structure, where the paired in-plane nitroxides lie in the trans position with respect to the bridging segment, and another structure, where the paired nitroxides lie in the cis position. The same cis-trans ambiguity holds for the structure solution found for BR1. The definitive choice between these two structures would require accurate quantum chemical calculations of their spin-density distributions, for example, by using DFT theory. Such an evaluation of  $\langle r_{AB}^{-3} \rangle$ , averaged over the spin density distributions, should differ for cis- and trans-conformations and would result in different  $\nu_{\parallel}$  values to be compared with the experimental values. However, a DFT refinement of our structure solution is beyond the scope of this work, which is focused on the more general aspects of the applicability of dipolar EPR spectroscopy to determine 3D molecular structures.

When discussing angular spin triangulation by combining nitroxide double spin labeling and high-field DS-EPR, one more important aspect should be considered: Inherently, each one of the paired nitroxides can serve either as a target or as an observer.

This raises the problem of how to distinguish them. The problem is not important for model nitroxide biradicals with a symmetric molecular structure. Then, it is not necessary to fix the observer and target frames because the polar angles,  $\phi$  and  $\eta$ , describing the direction of the dipolar vector in both frames, are equal. This allows for symmetry transformations, that is,  $\phi_A = \phi_B$ ;  $180^\circ - \phi_B$ ;  $180^\circ + \phi_B$ ;  $360^\circ - \phi_B$ , and the same transformations hold for  $\eta$ . However, in the case of doubly spin labeled macromolecules such as proteins, no symmetry can be expected. Therefore, not only all angles describing the geometry have to be determined but also the polar angles,  $\phi$  and  $\eta$ , have to be related to the nitroxide frames in specific spin-labeled positions. This can only be achieved if the two nitroxides in the pair can be distinguished spectroscopically. A spectroscopic distinction of the two nitroxides can be realized, for example, by asymmetric isotope substitution in the paired spin labels, for instance by substituting  $^{14}\text{N}$  for  $^{15}\text{N}$  in the observer radical. Then, its hyperfine structure is drastically different from that of the unsubstituted target radical. Unfortunately, it turned out that the superposition of two different hyperfine patterns renders the analysis of the multi-dimensional dipolar spectra even more difficult.

Another method for solving the problem of distinguishing between observer and target radicals is based on the specific electronic relaxation behavior of nitroxides. As is well-known, fluctuating hyperfine interactions of the unpaired electron with the proximate methylene protons of the nitroxide become time-dependent because of restricted rotation of the methyl groups and accelerate the relaxation decay of the echo signal.<sup>56,57</sup> The relaxation effect is temperature-dependent, and it can even suppress the echo signals within a specific temperature interval, resulting in the “blind window” between 120 and 160 K.<sup>58</sup> This will happen when the inverse correlation time of the methyl group rotations,  $\tau_c^{-1}$ , becomes comparable with the amplitude of hyperfine fluctuations,  $\delta A_{\text{Meth}}$ , that is, when  $\tau_c \times \delta A_{\text{Meth}} \approx 1$  holds. When, however, the methylene protons are substituted for deuterons,  $\delta A_{\text{Meth}}$  decreases, and the “blind window” shifts to a lower temperature. Consequently, if for the RIDME/PELDOR measurements only the observer spin label is deuterated and the target label remains protonated, at a properly chosen temperature the rotational relaxation will suppress solely the echo signals of the protonated nitroxides. Then, the observer-detected RIDME/PELDOR spectra should be recordable free from interfering target-detected contributions. Our test measurements have confirmed the feasibility of this approach.

The discussed strategies to disentangle the dipolar signals of doubly nitroxide spin-labeled systems are based on distinguishing the labeled sites by means of different magnetic or relaxation parameters. In this respect, a promising alternative to the paired nitroxides for high-field DS-EPR spectroscopy is to use, as one partner in the spin pair, the recently introduced  $\text{Gd}^{3+}$  spin tag<sup>22–24</sup> weakly interacting with a nitroxide partner<sup>25</sup> (see above). Properly designed high-field RIDME/PELDOR experiments on  $\text{Gd}^{3+}$ -nitroxide spin pairs are in the pipeline of this laboratory using the nitroxide label as the observer to determine the distance and the two polar angles which describe the position of the  $\text{Gd}^{3+}$  ion with respect to the nitroxide reference frame.

## 5. CONCLUSION

In this work we examined the capabilities and limitations of state-of-the-art electron-spin triangulation by dipolar EPR methodologies designed for 3D structure determination of

paramagnetic molecular complexes in disordered solids. In case of diamagnetic complexes, electron spin probes have to be introduced by chemical or molecular-biology techniques. Most commonly, nitroxide spin labels are used which are attached, for example, by SDSL. In particular, we discussed the angular triangulation approach, which extends the more common radial triangulation. It has become feasible by using dipolar EPR spectroscopy at high magnetic fields and correspondingly high microwave frequencies, for example, orientation-resolving RIDME and PELDOR at 3.4 T and 95 GHz. As test systems for determining the full 3D molecular structure, two nitroxide biradicals (pyrrolidine type BR1 and imidazoline type BR2) with rather stiff bridging blocks and deuterated nitroxide headgroups were chosen.

We show that the excellent detection sensitivity as well as the superior spectral and orientational resolution distinguish the high-field dipolar-EPR techniques as unique tools for 3D structure determination of large disordered biomacromolecular systems in solid solution. This holds true for both stable and short-lived transient molecular states, which compares favorably with other structure-determining magnetic-resonance methods, for example, solid-state NMR. Complementary to the established distance measurements for radial spin triangulation by SDSL+dipolar EPR methods, which preferably operate at lower field/frequency settings, angular spin triangulation by SDSL+high-field dipolar EPR has matured now to allow for 3D structure determination of disordered molecular systems that are selectively labeled with magnetically coupled electron spin pairs. Prominent applications include organic nitroxide biradicals and radical pairs in proteins.<sup>20,40,42,54,59</sup> Angular triangulation can be achieved with an experimental accuracy of better than  $\pm 5^\circ$ .<sup>20</sup> As compared to radial triangulation, angular triangulation requires only a significantly reduced number of base reference sites to be spin-labeled because of the reduction of necessary distance constraints. As a consequence, much less 2-fold labeled sample preparations are needed, which is another appealing aspect of the employment of high-field dipolar EPR methods for structure determination. It is anticipated that high-field pulsed dipolar EPR methods will become particularly important for studies of transient conformational changes of specific domains in proteins that occur in the course of biological function. Such studies do not require the solution of the complete 3D structure but can focus on detecting reaction-induced shifts of distances and orientations.

In conclusion, it should be emphasized that for the 3D structure determination of stable and short-lived radical-pair states of large molecular systems by high-field dipolar EPR spectroscopy the stage is set now for a wide range of applications in chemistry and molecular biology. The necessary high-field/high-frequency EPR instrumentation as well as the theoretical background for optimizing the data collection and spectral analysis have reached an adequate level of perfection for promising work in a fascinating area of the material and life sciences.

## ■ AUTHOR INFORMATION

### Corresponding Author

\*Address: Max-Planck-Institut für Bioanorganische Chemie, Stiftstrasse 34-36 5470, Mülheim an der Ruhr, Germany. Phone: 0049-208-3063555. Fax: 0049-208-3063955. E-mail: savitsky@mpi-muelheim.mpg.de.

## ■ ACKNOWLEDGMENT

We thank Yuri Grishin (Institute of Chemical Kinetics and Combustion, Novosibirsk, Russia) for enduring technical support, Martin Plato (FU Berlin, Germany) for helpful discussions concerning the quantum chemical data analysis, and Igor Grigorev (Institute of Organic Chemistry, Novosibirsk, Russia) for a gift of the BR2 nitroxide biradical. We gratefully acknowledge sustaining financial support by the Deutsche Forschungsgemeinschaft in the frame of the Priority Program SPP 1051 (“High-field EPR in Biology, Chemistry and Physics”), the Collaborative Research Center SFB 498 (“Protein–Cofactor Interactions in Biological Processes”), and the Group Project MO 132/19-2 (“Protein Action Observed by Advanced EPR”) as well as by the Max-Planck Society and the Free University Berlin.

## ■ REFERENCES

- (1) Fu, R. Q.; Cross, T. A. *Annu. Rev. Biophys. Biomol. Struct.* **1999**, 28, 235.
- (2) Hughes, C. E.; Baldus, M.; Franco, B.; Gerald, L. L.; Peter, W. Solid-State NMR Structural Studies of Proteins. In *Encyclopedia of Condensed Matter Physics*; Bassani, F., Liedl, G. L., Wyder, P., Eds.; Elsevier: Oxford, 2005; p 394.
- (3) Opella, S. J.; Marassi, F. M. *Chem. Rev.* **2004**, 104, 3587.
- (4) Cotten, M.; Soghomonian, V. G.; Hu, W.; Cross, T. A. *Solid-State Nucl. Magn. Reson.* **1997**, 9, 77.
- (5) Krushelnitsky, A.; Reichert, D. *Prog. Nucl. Mag. Res. Sp.* **2005**, 47, 1.
- (6) Sisamakis, E.; Valeri, A.; Kalinin, S.; Rothwell, P. J.; Seidel, C. A. M. Accurate single-molecule FRET studies using multiparameter fluorescence detection. In *Methods in Enzymology*, Vol 475: *Single Molecule Tools, Pt B*; Walter, N. G., Ed.; Academic Press: Burlington, 2010; Vol. 474; p 455.
- (7) Jeschke, G.; Bender, A.; Paulsen, H.; Zimmermann, H.; Godt, A. *J. Magn. Reson.* **2004**, 169, 1.
- (8) Schiemann, O.; Prisner, T. F. Q. *Rev. Biophys.* **2007**, 40, 1.
- (9) Tsvetkov, Y. D.; Milov, A. D.; Maryasov, A. G. *Russ. Chem. Rev.* **2008**, 77, 487.
- (10) Borbat, P. P.; Freed, J. H. Measuring distances by pulsed dipolar ESR spectroscopy: Spin-labeled histidine kinases. In *Methods in Enzymology*, Vol 423: *Two-Component Signaling Systems, B*; Simon, M., Crane, B., Crane, A., Eds.; Elsevier Academic Press, Inc: San Diego, 2007; Vol. 423; p 52.
- (11) Hubbell, W. L.; Altenbach, C. *Curr. Opin. Struct. Biol.* **1994**, 4, 566.
- (12) Hubbell, W. L.; Cafiso, D. S.; Altenbach, C. *Nat. Struct. Biol.* **2000**, 7, 735.
- (13) Banham, J. E.; Baker, C. M.; Ceola, S.; Day, I. J.; Grant, G. H.; Groenen, E. J. J.; Rodgers, C. T.; Jeschke, G.; Timmel, C. R. *J. Magn. Reson.* **2008**, 191, 202.
- (14) Jeschke, G.; Polyhach, Y. *Phys. Chem. Chem. Phys.* **2007**, 9, 1895.
- (15) Fajer, P. G.; Brown, L.; Song, L. Practical pulsed dipolar ESR(DEER). In *ESR Spectroscopy in Membrane Biophysics*; Hemminga, M. A., Berliner, L., Eds.; Springer: New York, 2007; Vol. 27, p 95.
- (16) Borbat, P. P.; McHaourab, H. S.; Freed, J. H. *J. Am. Chem. Soc.* **2002**, 124, 5304.
- (17) Weber, A.; Schiemann, O.; Bode, B.; Prisner, T. F. *J. Magn. Reson.* **2002**, 157, 277.
- (18) Schiemann, O.; Cekan, P.; Margraf, D.; Prisner, T. F.; Sigurdsson, S. T. *Angew. Chem., Int. Ed.* **2009**, 48, 3292.
- (19) Wegener, C.; Savitsky, A.; Pfeiffer, M.; Möbius, K.; Steinhoff, H. J. *Appl. Magn. Reson.* **2001**, 21, 441.
- (20) Savitsky, A.; Dubinskii, A. A.; Flores, M.; Lubitz, W.; Möbius, K. *J. Phys. Chem. B* **2007**, 111, 6245.
- (21) Flores, M.; Savitsky, A.; Paddock, M. L.; Abresch, E. C.; Dubinskii, A. A.; Okamura, M. Y.; Lubitz, W.; Möbius, K. *J. Phys. Chem. B* **2010**, 114, 16894.
- (22) Raitsimring, A. M.; Gunanathan, C.; Potapov, A.; Efremenko, I.; Martin, J. M. L.; Milstein, D.; Goldfarb, D. *J. Am. Chem. Soc.* **2007**, 129, 14138.
- (23) Potapov, A.; Yagi, H.; Huber, T.; Jergic, S.; Dixon, N. E.; Otting, G.; Goldfarb, D. *J. Am. Chem. Soc.* **2010**, 132, 9040.
- (24) Potapov, A.; Song, Y.; Meade, T. J.; Goldfarb, D.; Astashkin, A. V.; Raitsimring, A. *J. Magn. Reson.* **2010**, 205, 38.
- (25) Lueders, P.; Jeschke, G.; Yulikov, M. *J. Phys. Chem. Lett.* **2011**, 2, 604.
- (26) Möbius, K.; Savitsky, A. *High-Field EPR Spectroscopy on Proteins and their Model Systems: Characterization of Transient Paramagnetic States*; RSC Publishing: London, 2009.
- (27) Jeschke, G.; Sajid, M.; Schulte, M.; Ramezanian, N.; Volkov, A.; Zimmermann, H.; Godt, A. *J. Am. Chem. Soc.* **2010**, 132, 10107.
- (28) Godt, A.; Franzen, C.; Veit, S.; Enkelmann, V.; Pannier, M.; Jeschke, G. *J. Org. Chem.* **2000**, 65, 7575.
- (29) Grigorev, I. A.; Dikanov, S. A.; Shchukin, G. I.; Volodarskii, L. B.; Tsvetkov, Y. D. *J. Struct. Chem.* **1982**, 23, 870.
- (30) Savitsky, A.; Dubinskii, A. A.; Plato, M.; Grishin, Y. A.; Zimmermann, H.; Möbius, K. *J. Phys. Chem. B* **2008**, 112, 9079.
- (31) Savitsky, A.; Kuhn, M.; Duché, D.; Möbius, K.; Steinhoff, H. J. *J. Phys. Chem. B* **2004**, 108, 9541.
- (32) Kulik, L. V.; Dzuba, S. A.; Grigoryev, I. A.; Tsvetkov, Y. D. *Chem. Phys. Lett.* **2001**, 343, 315.
- (33) Milov, A. D.; Ponomarev, A. B.; Tsvetkov, Y. D. *Chem. Phys. Lett.* **1984**, 110, 67.
- (34) Milov, A. D.; Salikohov, K. M.; Shirov, M. D. *Fiz. Tverd. Tela* **1981**, 23, 975.
- (35) Pannier, M.; Veit, S.; Godt, A.; Jeschke, G.; Spiess, H. W. *J. Magn. Reson.* **2000**, 142, 331.
- (36) Kulik, L. V.; Paschenko, S. V.; Dzuba, S. A. *J. Magn. Reson.* **2002**, 159, 237.
- (37) Zaripov, R. B.; Dzhabarov, V. I.; Knyazev, A. A.; Galyametdinov, Y. G.; Kulik, L. V. *Appl. Magn. Reson.* **2011**, 40, 11.
- (38) Dubinskii, A. A.; Grishin, Y. A.; Savitsky, A. N.; Möbius, K. *Appl. Magn. Reson.* **2002**, 22, 369.
- (39) Jeschke, G.; Spiess, H. W. *Chem. Phys. Lett.* **1998**, 293, 9.
- (40) Socoli, G.; Argirevic, T.; Stubbe, J.; Tkach, I.; Bennati, M. *App. Magn. Reson.* **2010**, 37, 539.
- (41) Marko, A.; Margraf, D.; Cekan, P.; Sigurdsson, S. T.; Schiemann, O.; Prisner, T. F. *Phys. Rev. E* **2010**, 81, 021911.
- (42) Denysenkov, V. P.; Biglino, D.; Lubitz, W.; Prisner, T. F.; Bennati, M. *Angew. Chem., Int. Ed.* **2008**, 47, 1224.
- (43) Lovett, J. E.; Bowen, A. M.; Timmel, C. R.; Jones, M. W.; Dilworth, J. R.; Caprotti, D.; Bell, S. G.; Wong, L. L.; Harmer, J. *Phys. Chem. Chem. Phys.* **2009**, 11, 6840.
- (44) Pake, G. E. *J. Chem. Phys.* **1948**, 16, 327.
- (45) Jeschke, G.; Pannier, M.; Godt, A.; Spiess, H. W. *Chem. Phys. Lett.* **2000**, 331, 243.
- (46) Jeschke, G.; Koch, A.; Jonas, U.; Godt, A. *J. Magn. Reson.* **2002**, 155, 72.
- (47) Atherton, N. M. *Principles of Electron Spin Resonance*; Ellis Horwood: New York, 1993.
- (48) Bloess, A.; Möbius, K.; Prisner, T. F. *J. Magn. Reson.* **1998**, 134, 30.
- (49) Schweiger, A.; Jeschke, G. *Principles of Pulse Electron Paramagnetic Resonance*; University Press: Oxford, 2001.
- (50) Milov, A. D.; Ponomarev, A. B.; Tsvetkov, Y. D. *J. Struct. Chem.* **1984**, 25, 710.
- (51) Milov, A. D.; Naumov, B. D.; Tsvetkov, Y. D. *Appl. Magn. Reson.* **2004**, 26, 587.
- (52) Kulik, L. V.; Grishin, Y. A.; Dzuba, S. A.; Grigoryev, I. A.; Klyatskaya, S. V.; Vasilevsky, S. F.; Tsvetkov, Y. D. *J. Magn. Reson.* **2002**, 157, 61.
- (53) Jeschke, G.; Panek, G.; Godt, A.; Bender, A.; Paulsen, H. *Appl. Magn. Reson.* **2004**, 26, 223.
- (54) Polyhach, Y.; Godt, A.; Bauer, C.; Jeschke, G. *J. Magn. Reson.* **2007**, 185, 118.

- (55) Schweiger, A.; Gemperle, C.; Ernst, R. R. *J. Magn. Reson.* **1990**, 86, 70.
- (56) Barbon, A.; Brustolon, M.; Maniero, A. L.; Romanelli, M.; Brunel, L. *C. Phys. Chem. Chem. Phys.* **1999**, 1, 4015.
- (57) Dzuba, S. A.; Maryasov, A. G.; Salikhov, K. M.; Tsvetkov, Y. D. *J. Magn. Reson.* **1984**, 58, 95.
- (58) Zecevic, A.; Eaton, G. R.; Eaton, S. S.; Lindgren, M. *Mol. Phys.* **1998**, 95, 1255.
- (59) Denysenkov, V. P.; Prisner, T. F.; Stubbe, J.; Bennati, M. *Proc. Natl. Acad. Sci. U.S.A.* **2006**, 103, 13386.